Am J Physiol Lung Cell Mol Physiol 318: L226–L241, 2020.
First published November 6, 2019; doi:10.1152/ajplung.00123.2019.

RESEARCH ARTICLE | *Electronic Cigarettes: Not All Good News?*

Flavored e-liquids increase cytoplasmic Ca^{2+} levels in airway epithelia

Temperance R. Rowell,[1,2] James E. Keating,[3] Bryan T. Zorn,[1] Gary L. Glish,[3] Stephen B. Shears,[4] and Robert Tarran[1,2]

[1]*Marsico Lung Institute, University of North Carolina, Chapel Hill, North Carolina;* [2]*Department of Cell Biology and Physiology, University of North Carolina, Chapel Hill, North Carolina;* [3]*Department of Chemistry, University of North Carolina, Chapel Hill, North Carolina; and* [4]*Laboratory of Signal Transduction, National Institute of Environmental Health Sciences, Research Triangle Park, North Carolina*

Submitted 11 March 2019; accepted in final form 5 November 2019

Rowell TR, Keating JE, Zorn BT, Glish GL, Shears SB, Tarran R. Flavored e-liquids increase cytoplasmic Ca^{2+} levels in airway epithelia. *Am J Physiol Lung Cell Mol Physiol* 318: L226–L241, 2020. First published November 6, 2019; doi:10.1152/ajplung.00123.2019.—E-cigarettes are noncombustible, electronic nicotine-delivery devices that aerosolize an e-liquid, i.e., nicotine, in a propylene glycol-vegetable glycerin vehicle that also contains flavors. While the effects of nicotine are relatively well understood, more information regarding the potential biological effects of the other e-liquid constituents is needed. This is a serious concern, because e-liquids are available in >7,000 distinct flavors. We previously demonstrated that many e-liquids affect cell growth/viability through an unknown mechanism. Since Ca^{2+} is a ubiquitous second messenger that regulates cell growth, we characterized the effects of e-liquids on cellular Ca^{2+} homeostasis. To better understand the extent of this effect, we screened e-liquids for their ability to alter cytosolic Ca^{2+} levels and found that 42 of 100 flavored e-liquids elicited a cellular Ca^{2+} response. Banana Pudding (BP) e-liquid, a representative e-liquid from this group, caused phospholipase C activation, endoplasmic reticulum (ER) Ca^{2+} release, store-operated Ca^{2+} entry (SOCE), and protein kinase C (PKCα) phosphorylation. However, longer exposures to BP e-liquid depleted ER Ca^{2+} stores and inhibited SOCE, suggesting that this e-liquid may alter Ca^{2+} homeostasis by short- and long-term mechanisms. Since dysregulation of Ca^{2+} signaling can cause chronic inflammation, ER stress, and abnormal cell growth, flavored e-cigarette products that can elicit cell Ca^{2+} responses should be further screened for potential toxicity.

e-cigarette; ethyl maltol; ethyl vanillin; flavors; nicotine; tobacco; vanillin

INTRODUCTION

E-cigarettes are electronic nicotine-delivery systems that utilize a battery-powered coil to heat flavored e-liquids into an inhalable aerosol. E-liquids are usually composed of a propylene glycol-vegetable glycerin (PG/VG) base to which nicotine and a number of individual flavoring chemicals are added to create flavored e-liquids for purchase. E-cigarette use in adolescent populations has increased over time (4). Interestingly, the availability of flavors, especially sweet flavors, may contribute to e-cigarette use in youth and young adults (24). There are >400 different brands/vendors of flavored e-liquids in the United States alone (25). However, although e-liquids have been shown to be toxic in vitro, there is little information regarding underlying cellular mechanisms of toxicity, and e-cigarette health effects and safety are still widely debated (7, 49). Concern regarding inhalation safety for individual flavoring chemicals stems from cases of chronic diacetyl inhalation in manufacturing plant workers. Although diacetyl, a buttery flavor, is "generally recognized as safe" for ingestion, chronic inhalation can lead to the development of bronchiolitis obliterans or "popcorn lung," which is scarring and fibrosis of the airways (30). Interestingly, several recent studies have implicated flavored e-liquids and individual flavoring chemicals, in addition to PG/VG, in toxicity or alteration of other biological functions of respiratory cells (8, 22, 48, 50, 56). However, despite this emerging body of data, how e-liquids can exert their effects is not well understood.

Pulmonary epithelia are among the first lines of defense against inhaled toxicants. They serve as a physical barrier and are integral in coordinating innate defenses. Cellular Ca^{2+} plays important roles not only in normal lung physiology, but also in modulating immune cell activation and controlling the initiation and persistence of inflammation (27, 53). Typically, cells rely on a number of pumps, receptors, and channels to control fluctuations in cytosolic Ca^{2+} and sequester it into organelles to maintain low cytoplasmic Ca^{2+} levels under basal conditions (13). After activation, a subset of cell surface G protein-coupled receptors (GPCRs) activates phospholipase C (PLC) to generate inositol 1,4,5-triphosphate (IP_3). The subsequent stimulation of IP_3 receptors triggers endoplasmic reticulum (ER) Ca^{2+} release, followed by store-operated Ca^{2+} entry (SOCE) to replenish ER Ca^{2+} stores. SOCE requires the association of stromal interaction molecule 1 (STIM1) with Orai1 at ER-plasma membrane junctions; the resulting activation of Orai1 promotes Ca^{2+} entry (43). The signaling cascade continues downstream of SOCE to activate kinases such as protein kinase C (PKC). PKCα is canonically activated downstream of both PLC activation (i.e., diacylglycerol formation) and Ca^{2+} release (29, 57), and its activation in turn can cause cellular responses such as cell proliferation and apoptosis (36, 61). Inappropriate activation of these Ca^{2+}-signaling pathways can have profound effects on cell function and survival.

Using high-throughput screening approaches, we previously studied >200 e-liquids and found that many affected cell growth (48, 50). Given the number of flavored e-cigarettes that are commercially available, more information is needed regarding their potential cellular effects. Here, we tested the

Address for reprint requests and other correspondence: R. Tarran, 125 Mason Farm Rd., Marisco Hall, CB 7248, Chapel Hill, NC 27599 (e-mail: robert_tarran@med.unc.edu).

effects of commercially available e-liquids for their ability to alter an important universal cell-signaling pathway that can modulate cell growth/survival (i.e., cytosolic Ca^{2+}).

METHODS AND MATERIALS

Flavored E-cigarette liquids and aerosol exposure. E-liquids were purchased from The Vapor Girl (www.thevaporgirl.com) and NJOY (www.njoy.com/e-juice) (Table 1). The composition of each liquid, as measured by GC-MS, is shown in the online supplement (all Supplemental material is available at https://doi.org/10.15139/S3/UDSIGO). Experiments using the Banana Pudding e-liquid (BP) were performed from two different lots that were verified for chemical composition by GC-MS using the methods described below and to ensure consistency of the cytosolic Ca^{2+} responses. BP with and without 12 mg/ml nicotine was purchased. In addition to nicotine, BP also contained the following chemicals: 4H-pyran-4-one, 2-ethyl-3-hydroxy- [Chemical Abstracts Service (CAS) no. 4940-11-8], 5-thiazoleethanol, 4-methyl- (CAS no. 137-00-8), acetic acid, methyl ester (CAS no. 79-20-9), benzyl alcohol (CAS no. 100-51-6), ethyl vanillin (CAS no. 121-32-4), glycerin (CAS no. 56-81-5), phenol, 2-methoxy- (CAS no. 90-05-1), propylene glycol (CAS no. 57-55-6), pyridine, 3-(1-methyl-2-pyrrolidinyl)-, (S)- (CAS no. 54-11-5), vanillin (CAS no. 121-33-5), and vanillin propylene glycol acetal (CAS no. 68527-74-2). The e-liquid vehicle was advertised as 55:45 PG/VG. Thus a vehicle control was made in our laboratory using 55:45 PG/VG; both PG and VG were obtained from Sigma-Aldrich. Nicotine concentrations for each flavored e-liquid are listed in Table 1. The composition of each liquid, as measured by GC-MS, is shown in the online supplement.

GC-MS analysis of e-liquids. Qualitative e-liquid analysis was performed on a GC-triple-quadrupole MS (EVOQ 456GC-MS, Bruker, Billerica, MA) using a 0.25-mm ID, 0.25-μm-film capillary column (model DB-5MS, Agilent Technologies, Santa Clara, CA) and helium carrier gas (99.999% purity), as described elsewhere (48, 50). Injections (1 μL) were performed using an autosampler (model CP-8400, Bruker) with an injector temperature of 270°C. The GC oven was programmed with a 12.5-min temperature gradient (60–250°C), and the transfer line and electron ionization source were held at 250°C. Samples were prepared by dilution of 50 μL of e-liquid in 1 mL of methanol (optima grade) and vortexed for 30 s. Full-scan mass spectra were acquired from *m/z* 40–500. The National Institute for Standards and Technology 2014 mass spectral database (Gaithersburg, MD) and automated mass spectral deconvolution and identification system chromatography software were used to identify compounds.

Chemicals and reagents. PG, VG, DMSO, human placental type VI collagen, probenecid, thapsigargin, methanol, uridine triphosphate (UTP), and carbonyl cyanide *m*-chlorophenyl hydrazine (CCCP) were purchased from Sigma-Aldrich; DAPI, fura 2-AM, fluo 4-AM, rhod 2-AM, and Lipofectamine 2000 from Thermo Fisher; paraformaldehyde (PFA) from Affymetrix; and 2-aminoethoxydiphenyl borate (2-APB) from Tocris. DAPI, thapsigargin, fura 2-AM, fluo 4-AM, and rhod 2-AM were reconstituted using DMSO and applied to cells in experiments where the final DMSO concentration was ≤0.1%. STIM1 tagged with mCherry on the COOH terminus was kindly provided by Dr. Ricardo Dolmetsch (39). Orai1 tagged with yellow fluorescent protein (YFP) on the COOH terminus was purchased from Addgene (catalog no. 19756) (42).

Cell culture and transfections. Procurement of primary human bronchial epithelial cells (HBECs) from nonsmoker human excess donor lungs was approved by the University of North Carolina Institutional Review Board (protocol 03-139), as described previously (44). HBECs were grown on glass coverslips coated with human placental type VI collagen, cultured in bronchial epithelial growth medium with 5% CO_2 at 37°C, and assayed within 1 wk of plating. CALU3 cells were cultured in minimum essential medium-α with 10% FBS and penicillin-streptomycin (Gibco) with 5% CO_2 at 37°C. CALU3 cells were seeded onto glass coverslips for fura 2 experiments and 12- or 96-well plastic dishes (Corning) for all other experiments. HEK-293T cells were cultured in DMEM (high-glucose) with 10% FBS and penicillin-streptomycin (Gibco) with 5% CO_2 at 37°C. HEK-293T cells were plated onto glass coverslips for fura 2 and STIM1/Orai1 puncta-imaging experiments. HEK-293T cells were seeded into 12- and 24-well plastic dishes (Corning) for fluo 4 and total inositol phosphate activation experiments.

Ca^{2+} signaling. HBECs and CALU3 cells were loaded with 8 μM fura 2-AM in the presence of 1–2.5 mM probenecid for 40 min at 37°C before experiments. HEK-293T cells were loaded with 5 μM fura 2-AM for 20 min at 37°C before experiments. All cultures were rinsed with PBS and replaced with a standard Ringer solution, as described previously (45). Fura 2 fluorescence intensities were measured every 15 or 30 s using a ×40 magnification 1.3-numerical aperture (NA) oil-immersion objective on a Nikon Ti-S inverted microscope with alternating excitation at 340 and 380 nm (emission; excitation >450 nm) using Ludl filter wheels at room temperature. Images were captured with an Orca charge-coupled device camera (Hammamatsu) and analyzed using HCImage software. All fura 2 intensities were background-subtracted and divided to obtain the ratio (i.e., 340-nm signal/380-nm signal) and then normalized to the starting ratio to yield R/R_0 measurements. Thapsigargin was added to cultures at a final concentration of 2 μM. In some cases, nominally Ca^{2+}-free Ringer solution was added extracellularly, as described elsewhere (45). For experiments in 96-well plates, CALU3 and HEK-293T cells were loaded with fluo 4-AM, as described for fura 2. Fluorescence intensities were measured every 15 or 30 s using a Tecan Infinite Pro plate reader (excitation: 490 ± 10 nm; emission: 516 ± 5 nm) at room temperature. Changes in fluo 4 fluorescence were normalized to the baseline (F/F_0) after subtraction of background light levels. Traces were plotted to show F/F_0 over time, and the peak change in F/F_0 was measured for each dose and compared between treatments. Thapsigargin was added to cultures at a final concentration of 2 μM. Neat e-liquids were diluted in Ringer solution and exposed to cells at final concentration (%vol/vol). CALU3 cells were pretreated with 10 μM CCCP for 1 h at 37°C (see Fig. 5, *C* and *D*). HEK-293T cells were pretreated with 100 μM 2-APB for 1 min before UTP or e-liquid treatment (see Fig. 6*D*).

Changes in mitochondrial Ca^{2+} were measured in CALU3 cells with or without CCCP pretreatment. Cells were loaded with 3 μM rhod 2 for 1 h at 37°C, rinsed with PBS, and incubated in medium for 12–24 h, as described elsewhere (45). Cultures were rinsed, and medium was replaced with a standard Ringer solution. Fluorescence intensities were measured

Table 1. *Flavored e-liquids used in the fluo 4 Ca^{2+} screen from Fig. 1*

e-Liquid Flavor	Peak Ca^{2+} Response		*P* Value	Vendor	Nicotine, mg/ml
	Mean	SE			
0% e-liquid (control)	1.080	0.06	N/A	N/A	0
3% PG/VG (vehicle)	1.372	0.07	>0.9999	Sigma	0
Arctic Tobacco	10.832	0.52	<0.0001	The Vapor Girl	12
Menthol	8.703	0.46	<0.0001	NJOY	10
Hot Cinnamon Candies	6.780	0.69	<0.0001	The Vapor Girl	12
Peach Tea	6.124	0.87	<0.0001	NJOY	10
Cool Mint	3.927	0.36	<0.0001	The Vapor Girl	12
Banana Pudding	3.216	0.37	<0.0001	The Vapor Girl	12
Banana Pudding	3.193	0.22	<0.0001	The Vapor Girl	0
Valkyrie	3.002	0.46	<0.0001	The Vapor Girl	12
Black Coffee	2.710	0.29	<0.0001	The Vapor Girl	12
Biscotti	2.605	0.25	<0.0001	The Vapor Girl	12
Caramel Corn Crunch	2.525	0.14	<0.0001	The Vapor Girl	12
Chocolate Tobacco Heaven	2.350	0.18	<0.0001	The Vapor Girl	12
Candy Corn	2.282	0.12	<0.0001	The Vapor Girl	12
Key Lime Pie	2.182	0.11	<0.0001	The Vapor Girl	12
Caramel Apple	2.172	0.08	<0.0001	The Vapor Girl	12
Captain Suckle	1.994	0.08	0.0003	The Vapor Girl	12
Cheesecake with Graham Cracker	2.086	0.10	0.0004	The Vapor Girl	12
Cinnamon Roll	2.098	0.15	0.0006	The Vapor Girl	12
Strawberry Mango Smoothie	2.180	0.20	0.0007	The Vapor Girl	12
Missed Her Cookie	2.132	0.15	0.0007	The Vapor Girl	12
Chocolate Pecan Fudge	2.118	0.15	0.0007	The Vapor Girl	12
Apple Pie	2.082	0.12	0.0007	The Vapor Girl	12
Candy Cane	1.994	0.03	0.0007	The Vapor Girl	12
Circus Guava	2.128	0.21	0.0008	The Vapor Girl	12
Chocolate Banana	2.074	0.13	0.0009	The Vapor Girl	12
Angel Lust	1.989	0.09	0.0009	The Vapor Girl	12
Tiramisu	1.996	0.10	0.0015	The Vapor Girl	12
Dulce de Leche	1.971	0.11	0.0019	The Vapor Girl	12
Kola	3.226	0.82	0.0027	The Vapor Girl	12
RY4 Doubler	1.960	0.16	0.0048	The Vapor Girl	12
Pumpkin Pie	2.270	0.28	0.0056	The Vapor Girl	12
Chocolate Dipt Raspberry	1.891	0.11	0.0089	The Vapor Girl	12
Double Espresso	1.891	0.17	0.0096	NJOY	10
Honey Vanilla Tobacco	1.854	0.10	0.0155	The Vapor Girl	12
DB's Dessert	1.818	0.08	0.0180	The Vapor Girl	12
Chocolate Moo	1.949	0.19	0.0184	The Vapor Girl	12
Bavarian Crème Donut	1.801	0.11	0.0336	The Vapor Girl	12
Sweet Potato Pie	1.784	0.08	0.0339	The Vapor Girl	12
Lemon Meringue Pie	1.853	0.15	0.0350	The Vapor Girl	12
Sugar Cookie	1.787	0.10	0.0398	The Vapor Girl	12
Butterscotch	1.784	0.11	0.0461	The Vapor Girl	12
Black Cherry	1.765	0.08	0.0461	The Vapor Girl	12
Marshmallow	1.729	0.07	0.0781	The Vapor Girl	12
Crispy Melon	1.742	0.09	0.0785	The Vapor Girl	12
Strawberry Pop O'Tarts	1.701	0.08	0.1204	The Vapor Girl	12
Vanilla Custard	1.696	0.05	0.1251	The Vapor Girl	12
Chocolate Fudge	1.675	0.07	0.1322	The Vapor Girl	12
Buttery Nipple	1.718	0.12	0.1420	The Vapor Girl	12
Menthol Tobacco	1.911	0.32	0.1727	The Vapor Girl	12
Chai Latte	1.669	0.12	0.2911	The Vapor Girl	12
Bubble Gum	1.691	0.15	0.3984	The Vapor Girl	12
Arctic Raspberry	1.652	0.12	0.4539	The Vapor Girl	12
Blueberry Cinnamon Streusel Muffin	1.647	0.13	0.4544	The Vapor Girl	12
Slug Juice	1.610	0.09	0.5847	The Vapor Girl	12
Pillow Fight	1.596	0.07	0.6791	The Vapor Girl	12
Peach Piano	1.597	0.04	0.6970	The Vapor Girl	12
Root Beer	1.560	0.07	0.9216	The Vapor Girl	12
Cuba Libre	1.564	0.09	>0.9999	The Vapor Girl	12
Black Dragon	1.563	0.09	>0.9999	The Vapor Girl	12
Black Thorn	1.562	0.09	>0.9999	The Vapor Girl	12
Orphan Tears	1.562	0.08	>0.9999	The Vapor Girl	12
Coconut Rum	1.552	0.08	>0.9999	The Vapor Girl	12
Banana	1.527	0.05	>0.9999	The Vapor Girl	12
Chai	1.525	0.10	>0.9999	The Vapor Girl	12
Coconut Water	1.501	0.08	>0.9999	The Vapor Girl	12

Continued

Table 1.—*Continued*

e-Liquid Flavor	Peak Ca^{2+} Response		*P* Value	Vendor	Nicotine, mg/ml
	Mean	SE			
Desert Cow	1.500	0.18	>0.9999	The Vapor Girl	12
Cherry Kola	1.499	0.06	>0.9999	The Vapor Girl	12
RY4 Classic	1.498	0.07	>0.9999	The Vapor Girl	12
Cat Nip	1.477	0.09	>0.9999	The Vapor Girl	12
Clove Cigar	1.470	0.13	>0.9999	The Vapor Girl	12
Bubbly Berry	1.470	0.07	>0.9999	The Vapor Girl	12
Butter Crunch	1.455	0.10	>0.9999	NJOY	10
Alchemy	1.444	0.08	>0.9999	The Vapor Girl	12
Cotton Berry	1.429	0.06	>0.9999	The Vapor Girl	12
French Vanilla Hazelnut Espresso	1.418	0.10	>0.9999	The Vapor Girl	12
Mt. DUDE	1.412	0.04	>0.9999	The Vapor Girl	12
Black and Blue Berries	1.408	0.09	>0.9999	NJOY	10
Kiwi Blast	1.402	0.12	>0.9999	The Vapor Girl	12
Icy Blast	1.397	0.06	>0.9999	The Vapor Girl	12
Strawberries and Champagne	1.389	0.08	>0.9999	The Vapor Girl	12
Single Malt Scotch	1.313	0.06	>0.9999	NJOY	10
Blue Pom	1.279	0.06	>0.9999	The Vapor Girl	12
Watermelon	1.268	0.06	>0.9999	The Vapor Girl	12
Pomegranate	1.266	0.11	>0.9999	NJOY	10
Pixie Dust	1.256	0.08	>0.9999	The Vapor Girl	12
Blue Moo	1.249	0.03	>0.9999	The Vapor Girl	12
Blood Orange	1.247	0.04	>0.9999	NJOY	10
Vanilla Bean	1.238	0.08	>0.9999	NJOY	10
Arctic Strawberry	1.237	0.04	>0.9999	The Vapor Girl	12
Bartlett Pear	1.207	0.03	>0.9999	The Vapor Girl	12
Grape Soda	1.201	0.09	>0.9999	The Vapor Girl	12
Raspberry	1.195	0.05	>0.9999	The Vapor Girl	12
Classic Tobacco	1.192	0.05	>0.9999	NJOY	10
Grape!	1.190	0.03	>0.9999	The Vapor Girl	12
Bahama Mama	1.174	0.04	>0.9999	The Vapor Girl	12
Sour Fruit Punch	1.149	0.05	>0.9999	The Vapor Girl	12
Black Peppercorn	1.134	0.05	>0.9999	The Vapor Girl	12
Captain Zach Cigar	1.098	0.06	>0.9999	The Vapor Girl	0
Cranberry Crunch	1.074	0.04	>0.9999	The Vapor Girl	12
Cranberry Delight	1.058	0.03	>0.9999	The Vapor Girl	12

PG/VG, polyethylene glycol-vegetable glycerin.

every 15 or 30 s using a Tecan Infinite Pro plate reader (ex: 550 ± 5 nm; em: 580 ± 5 nm) at room temperature. Changes in rhod 2 fluorescence were plotted as peak changes in fluorescence intensity after subtraction of background light levels.

Aerosol exposures. E-cigarette aerosols were generated as previously described (15, 50). Briefly, we used a Sigelei FuChai 200-W device with a Crown stainless steel subtank and a 0.25-Ω SUS316 dual coil (Uwell, City of Industry, CA). Aerosols were generated by activating the e-cigarette device and drawing the liquid into a 100-mL syringe from the mouthpiece of the subtank. Based on existing vaping topography (31, 33), we generated 70-mL puffs drawn over 3 s at 100 W. To directly vape into 96-well plates, we used a three-dimensional printed manifold, as previously described (15). These manifolds were used to simultaneously vape six wells per plate. We have shown that e-liquids are autofluorescent, and using autofluorescence as an indicator of deposition, we previously found that our vaping approach in 96-well plates resulted in an even deposition of e-liquid vapor that was highly reproducible (15). CALU3 cells were seeded into 96-well plates and loaded with fluo 4-AM before exposure. Cells were submerged in 100 μL of Ringer solution per well, and baseline fluorescence was measured for 1 min before cells were moved to a dark chemical hood and exposed to 0–25 puffs of air or heated aerosols. Naïve wells were studied on each plate in parallel and were covered with silicone strips to avoid unwanted aerosol exposures. After the exposure, plates were returned to the plate reader, and fluorescence was read over time at 37°C.

Total cell number (DAPI). As an indicator of total cell number, cultures were fixed with 100% methanol for 10 min at room temperature, rinsed with PBS, and stained with DAPI (1:1,000 dilution) for 5–10 min. DAPI fluorescence was measured using a Tecan Infinite Pro plate reader (ex: 360 ± 5 nm; em: 460 ± 5 nm) at room temperature (48).

Measurement of total intracellular inositol phosphate. HEK-293T cells were cultured in 24-well plates for 6 h before an 18-h incubation with [^{3}H]inositol (4 μCi/ml; American Radiolabeled Chemicals, St. Louis, MO) in culture medium. Cells were then rinsed and incubated in fresh medium (in mM: 115 NaCl, 25 HEPES, 10 glucose, 5 KCl, 1.35 $CaCl_2$, 1 NaH_2PO_4, and 0.5 $MgSO_4$) for 2 h at 37°C. LiCl (10 mM) was added to each culture before the experiment was initiated, and cells were exposed to buffer only, 200 μM UTP, 3% PG/VG, 3% BP (12 mg/ml nicotine), or 3% BP (0 mg/ml nicotine) for 2 min. Assays were quenched by aeration of the medium and addition of 0.4 mL of ice-cold 2 M perchloric acid-0.2 mg/ml inositol phosphate. Cultures were left on ice for 10 min before the medium was transferred to microcentrifuge tubes and neutralized with 1 M KCO_3 and 40 mM EDTA. Samples were left overnight at 4°C, and perchlorate precipitate was removed via

centrifugation. Gravity-fed ion-exchange chromatography was used to separate [^{3}H]inositol (Ins) from the total fraction of [^{3}H]inositol-labeled inositol phosphates ("InsP": i.e., $InsP_1$ + $InsP_2$ + $InsP_3$ + $InsP_4$) (54). Data were calculated as 1,000 × (InsP/Ins) and then transformed to percent activation at 2 min for each experiment

$$\%\text{activation} = \frac{\text{experimental value} - \text{average PG/VG value}}{\text{average PG/VG value}} * 100$$

E-liquid internalization imaging. CALU3 cells were plated onto glass coverslips. Medium was rinsed and replaced with Ringer solution before imaging. All imaging was conducted on a Leica SP8 confocal microscope with a ×63 magnification 1.4 NA oil-immersion objective. Bright-field and fluorescence (ex: 405 nm; em: 460 nm) images were taken before and after cells were exposed to BP.

STIM1 and Orai1 puncta quantification. HEK-293T cells were plated onto glass coverslips and transfected with Orai1-YFP and STIM1-mCherry using Lipofectamine 2000 according to the manufacturer's protocol, as described previously (55). Cells expressing STIM1-mCherry or Orai1-YFP were treated with 0% BP (medium), 3% PG/VG, 2 μM thapsigargin, 3% BP (0 mg/ml nicotine), or 3% BP (12 mg/ml nicotine) for 5–10 min. Cells were fixed with 4% PFA for 10 min after treatment and rinsed with PBS before imaging. All puncta imaging was conducted on a Leica SP8 confocal microscope with a ×63 magnification 1.4 NA oil-immersion objective. Multiple images were taken per coverslip from different parts of the coverslip, and ≥12 transfected cells were visually analyzed for the percentage of puncta-positive cells per coverslip.

Immunoblots. Rabbit anti-phosphorylated PKCα and anti-PKCα (both diluted 1:1,000) were purchased from Abcam, mouse anti-GAPDH (diluted 1:1,000) from Santa Cruz Biotechnology, and peroxidase-conjugated rabbit or mouse (both diluted 1:3,000) from Jackson ImmunoResearch. CALU3 cells were plated in 60-mm dishes and exposed to 3% BP (12 mg/ml nicotine) for 0–60 min. Cells were lysed in modified Pierce immunoprecipitation lysis buffer with 25 mM Tris·HCl (pH 7.4), 150 mM NaCl, 1% NP-40, and 1 mM EDTA and supplemented with 1× proteinase inhibitor cocktail and 1× phosphatase inhibitor cocktail (Roche) to detect protein expression from total cell lysates. Lysates were processed by sodium dodecyl sulfate-polyacrylamide gel electrophoresis and immunoblotting.

Heatmap of peak cytosolic Ca^{2+} screen. Peak cytosolic Ca^{2+} responses of 100 flavored e-liquids were measured and compared with the 0% e-liquid control. Statistically significant responses ($P < 0.05$) were $\log_2$-transformed, and a heatmap was generated using Morpheus software (Broad Institute).

E-liquid chemical constituent analysis from cytosolic Ca^{2+} screen. A Random Forest classification model using R version 3.4.1 was used to predict whether significant cytosolic Ca^{2+} responses in cell cultures could be determined using qualitative GC-MS chemical constituent presence/absence data, as well as the sum of all chemicals within each e-liquid, as input features. The model ($n = 100$) used a randomly sampled training set (70%) in which the remaining data were used as a test set using 10,001 decision trees. The mtry parameter was determined by using the lowest out-of-bag error rate resulting from tuneRF with stepFactor = 0.85, ntreeTry = 10,001, improve = 0.005. The Random Forest models were repeated using 10 seeds.

Statistical analyses. Unless noted, all statistics were performed using Prism GraphPad software (San Diego, CA). All data were shown as means ± SE. Data were analyzed using the Kruskal-Wallis test with Dunn's multiple-comparisons test or the Mann-Whitney test as appropriate. $P \leq 0.05$ was judged as significant. All experiments were performed on at least three separate occasions. HBECs were cultured from three or more normal, nonsmoker donors. We used the Random Forest model in the "mobForest" package for R software to compare individual e-liquid chemical components vs. the effect of each e-liquid on cytoplasmic Ca^{2+} (21). The Mean Decrease in Gini, which is an indicator of a variable's importance for estimating a target variable, was used to assess data quality in the Random Forest model. The Mean Decrease in Gini was defined as the mean of a variable's total decrease in node impurity, weighted by the proportion of samples reaching that node in each individual decision tree in the Random Forest model.

RESULTS

Acute e-liquid addition elicits cytosolic Ca^{2+} responses in CALU3 cells. Since Ca^{2+} is an important intracellular second messenger, we screened 100 flavored e-liquids from local and national vendors to see if they could affect cytoplasmic Ca^{2+} levels. We cultured CALU-3 cells in 96-well plates for 24 h, loaded them with the Ca^{2+}-sensitive dye fluo 4, and acutely exposed them to e-liquids. We found that 42 of 100 flavored e-liquids elicited a significant increase in cytosolic Ca^{2+} compared with the 0% e-liquid control (Fig. 1*A*). We previously analyzed >200 e-liquids by GC-MS (48, 50), and the chemical composition data are accessible online at www.eliquidinfo.org. To better understand why a diverse number of e-liquids might be able to elicit a cytosolic Ca^{2+} signal, these data were used to compare e-liquids for chemical composition relative to their cytosolic Ca^{2+} response. We used a model-based recursive partitioning method to make predictions based on these parameters using the Random Forest model (21). According to this approach, the average accuracy of correctly classified e-liquids was 75%, suggesting that qualitative constituent data may be able to predict cytosolic Ca^{2+} signaling (Fig. 1*B*). Using the Random Forest model, the Mean Decrease in the Gini Index is used to measure the degree to which the predictive variables (in this case, e-liquid chemical composition) can predict the outcome (i.e., changes in Ca^{2+}). The total number of chemicals in each e-liquid had the highest Mean Decrease in the Gini Index, suggesting that the more chemicals in an e-liquid, the more likely it was to elicit a Ca^{2+} response (Fig. 1*B*). However, ethyl vanillin (CAS no. 121-32-4), ethyl maltol (CAS no. 4940-11-8), and vanillin (CAS no. 121-33-5) also showed high Mean Decreases in the Gini Index and were also considered to be major variables in classification (Fig. 1*B*).

BP acutely elevates cytosolic Ca^{2+} in multiple cell types. We previously showed that BP inhibited cell growth (48). Since BP elicited an increase in Ca^{2+} (Fig. 1*A*, Table 1) and also contained ethyl vanillin, ethyl maltol, and vanillin, we chose it as a representative e-liquid for more detailed study. We loaded cells with a cytosolic Ca^{2+} indicator (fura 2 or fluo 4) and exposed them to BP diluted in Ringer solution. We

Fig. 1. Multiple flavored e-liquids elevate cytosolic Ca^{2+} levels. CALU3 cells were seeded into 96-well plates and loaded with fluo 4. Cells were challenged with 3% flavored e-liquids, and peak Ca^{2+} responses were compared. Peak Ca^{2+} responses are shown in the heatmap and reported in Table 1. *A*: all significant responses (n = 42) were log_2-transformed and plotted on a heatmap (n = 7–12 wells per treatment). Doses were compared with their 0% e-liquid controls. F/F_0, fluorescence ratio. *B*: heatmap showing the top-28 factors/chemicals' Mean Decrease in Gini Index, as a measure of a variable's importance for estimating a target variable, averaged across 10 Random Forest classifiers (n = 100). Mean change in fluo 4 fluorescence, as well as vendor information for each e-liquid, is shown in Table 1, and the composition of each e-liquid can be found in the online supplement https://doi.org/10.15139/S3/UDSIGO.

found an increase in cytosolic Ca^{2+} in primary HBECs, CALU3 cells, and HEK-293T cells after BP addition (Fig. 2, *A–C*). An additional 3% PG/VG vehicle control run in CALU3 and HEK-293T cells did not elicit a response. Peak responses to each treatment per cell type were compared (Fig. 2*D*). Thapsigargin is a sarco/endoplasmic reticulum Ca^{2+}-ATPase (SERCA) pump inhibitor that depletes ER stores to activate SOCE (34). Addition of 3% BP diminished the response to thapsigargin, suggesting that BP caused ER Ca^{2+} release (Fig. 2, *A–D*). BP used in Fig. 2, *A–D*, contained 12 mg/ml nicotine. To control for the potential effects of nicotine, a separate BP that contained 0 mg/ml nicotine was purchased. CALU3 cultures were treated with 3% BP with or without 12 mg/ml nicotine, and the cytosolic Ca^{2+} responses were measured over time. The changes in fluo 4 fluorescence are shown in Fig. 2*E* for BP with 12 mg/ml nicotine and in Fig. 2*F* for BP without nicotine. BP caused a peak fluo 4 response that was not affected by nicotine or by washout (Fig. 2*G*). In contrast, the plateau phase was diminished in the absence of nicotine (Fig. 2*H*). Moreover, only BP that contained 12 mg/ml nicotine was affected by the washout protocol (Fig. 2*H*), suggesting that nicotine contributed to the plateau, but not the peak, phase.

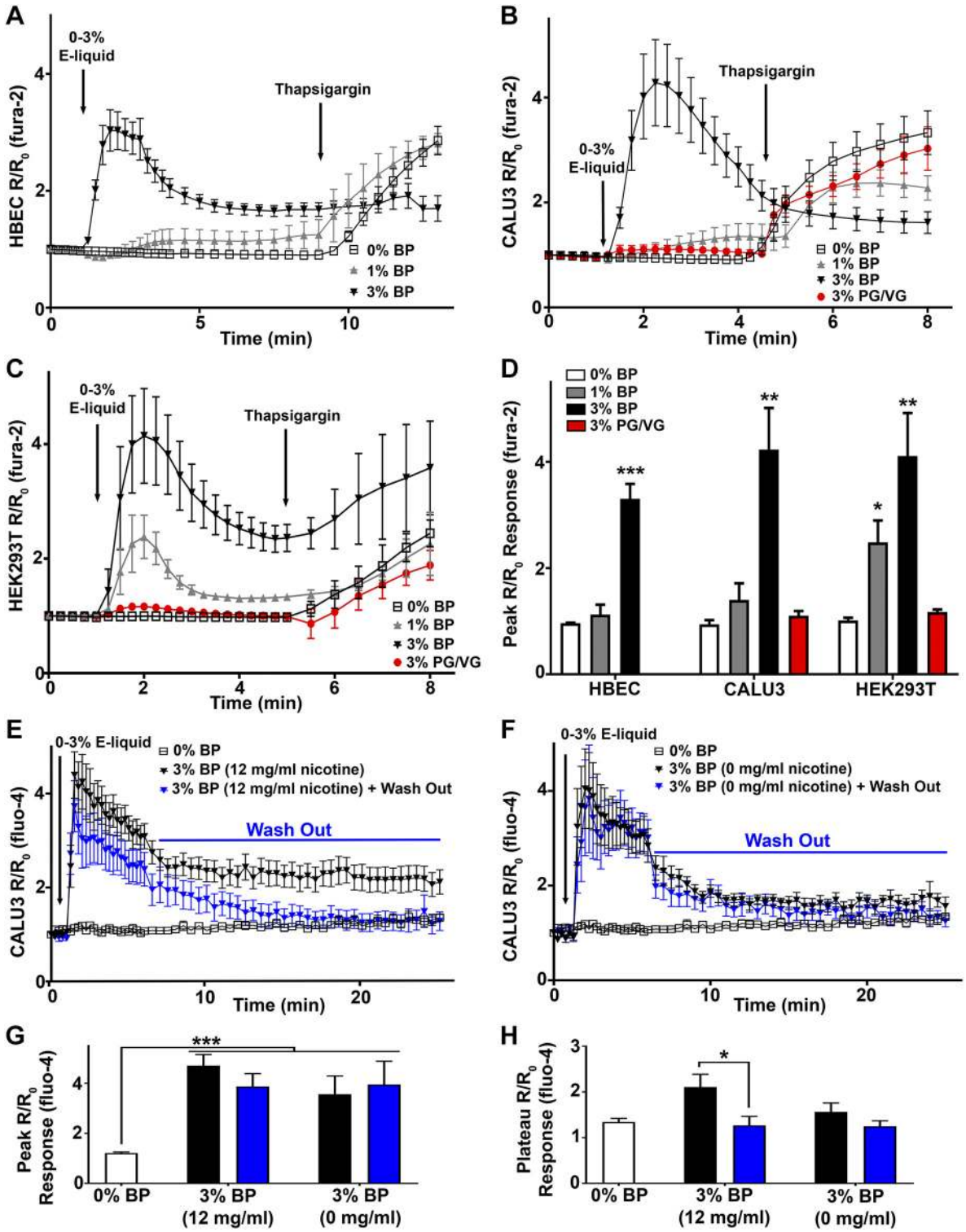

Fig. 2. Banana Pudding e-liquid (BP) acutely elevates cytoplasmic Ca^{2+} in primary and immortalized epithelia. Primary human bronchial epithelial cells (HBECs), CALU3 cells, and HEK-293T cells were plated on glass coverslips and loaded with the Ca^{2+} indicator fura 2. Cells were challenged acutely with BP with or without nicotine or with the e-liquid vehicle polyethylene glycol-vegetable glycerin (PG/VG) diluted in Ringer solution followed by thapsigargin. *A–C*: Ca^{2+} signals were measured over time and reported as change in fluorescence relative to baseline (R/R_0). *D*: peak changes for each cell type in response to treatments. Additional CALU3 cells were loaded with the Ca^{2+} dye fluo 4. *E* and *F*: cells were exposed to BP with or without 12 mg/ml nicotine diluted in Ringer solution, and change in fluorescence was measured over time. For BP with nicotine only (▼), e-liquid was washed out (blue line). *G* and *H*: peak and plateau changes for each treatment measured at 1.5 and 25 min posttreatment respectively. Black bars, e-liquid present; blue bars, e-liquid washed out. Values are means ± SE; n = 4–11 coverslips per treatment (*A–D*) and 8–13 wells per treatment (*E* and *F*). $^*P < 0.05$, $^{**}P < 0.01$, $^{***}P < 0.001$ vs. control.

Vaped BP also elicits an acute cytosolic Ca^{2+} response. Since we found increases in cytosolic Ca^{2+} following direct BP exposure, we sought to determine whether aerosolized BP would also increase cytosolic Ca^{2+}. We loaded CALU3 cells with fluo 4 and measured cytosolic Ca^{2+} responses following exposure to BP aerosol. We elected to expose cells to 5–25 puffs, which was on the lower end, but still representative, of real-world vaping sessions in humans (23). Neither puffs of air nor PG/VG (vehicle) elicited a change in cytosolic Ca^{2+} (Fig. 3, *A* and *B*). In contrast, addition of thapsigargin elevated Ca^{2+}, suggesting that the cells were responsive to stimuli. However, exposure to 5–25 puffs of BP aerosol elicited robust and persistent increases in cytosolic Ca^{2+} and diminished the thapsigargin response, indicating that the ability of BP to affect thapsigargin-sensitive stores was maintained when cells were exposed to BP as an aerosol (Fig. 3, *C* and *D*).

Thapsigargin-induced Ca^{2+} release is diminished following BP exposure. Since BP dose dependently elicited acute increases in cytosolic Ca^{2+}, we next tested whether these effects persisted over time. Accordingly, we incubated CALU3 cells with 3% BP or PG/VG for 3 or 24 h and then measured the thapsigargin-stimulated Ca^{2+} response. After both 3 and 24 h of exposure to 3% BP, the response to thapsigargin was significantly attenuated. In contrast, 3 or 24 h of exposure to the PG/VG vehicle did not affect the thapsigargin response (Fig. 4, *A* and *B*). Some e-liquids are cytotoxic and decrease the number of cells in culture (48). To check whether prolonged BP exposure was cytotoxic, we stained cell nuclei with DAPI and measured the resultant fluorescence using a multiplate reader. Total DAPI fluorescence was not different across groups, indicating that chronic BP exposure did not decrease total cell number (Fig. 4*C*). We then performed a 24-h washout with culture medium to test whether the thapsigargin response could be restored after chronic BP exposure. Indeed, the thapsigargin response was restored following washout (Fig. 4, *D* and *E*), and there was no decrease in DAPI staining with BP or PG/VG cultures compared with the vehicle control (Fig. 4*F*).

BP induces ER Ca^{2+} release/SOCE and does not involve mitochondrial Ca^{2+}. Ca^{2+} is sequestered into multiple intracellular stores, including the ER, to maintain low Ca^{2+} levels under basal conditions (18). Since cultures did not respond to

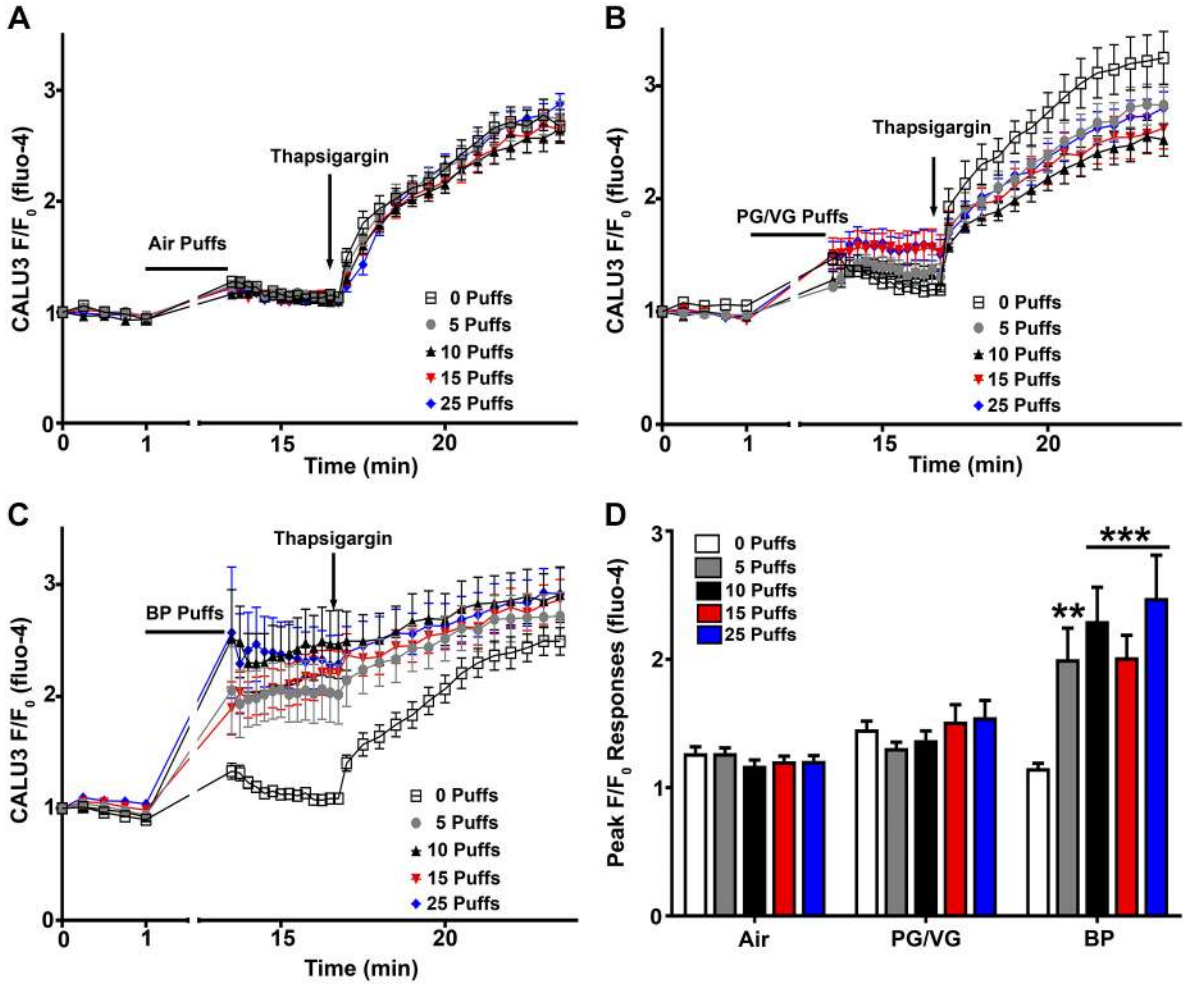

Fig. 3. Banana Pudding (BP) aerosol elicits acute, but persistent, increases in cytoplasmic Ca^{2+} in airway epithelia. CALU3 cells were seeded in 96-well plates. Cells were loaded with the Ca^{2+} indicator fluo 4, and medium was replaced with Ringer solution before baseline fluorescence was measured. *A–C*: cultures were exposed to puffs of air, polyethylene glycol-vegetable glycerin (PG/VG) aerosol, or BP aerosol. After puffs were administered, fluorescence was read at timed intervals following aerosol exposure and thapsigargin addition, and changes in fluorescence (F/F_0) were plotted over time. Both PG/VG (vehicle) and air puff exposures were performed as controls. *D*: peak changes in fluorescence over time. Values are means ± SE; n = 17–30 wells per treatment. $^{**}P < 0.01$, $^{***}P < 0.001$ vs. control.

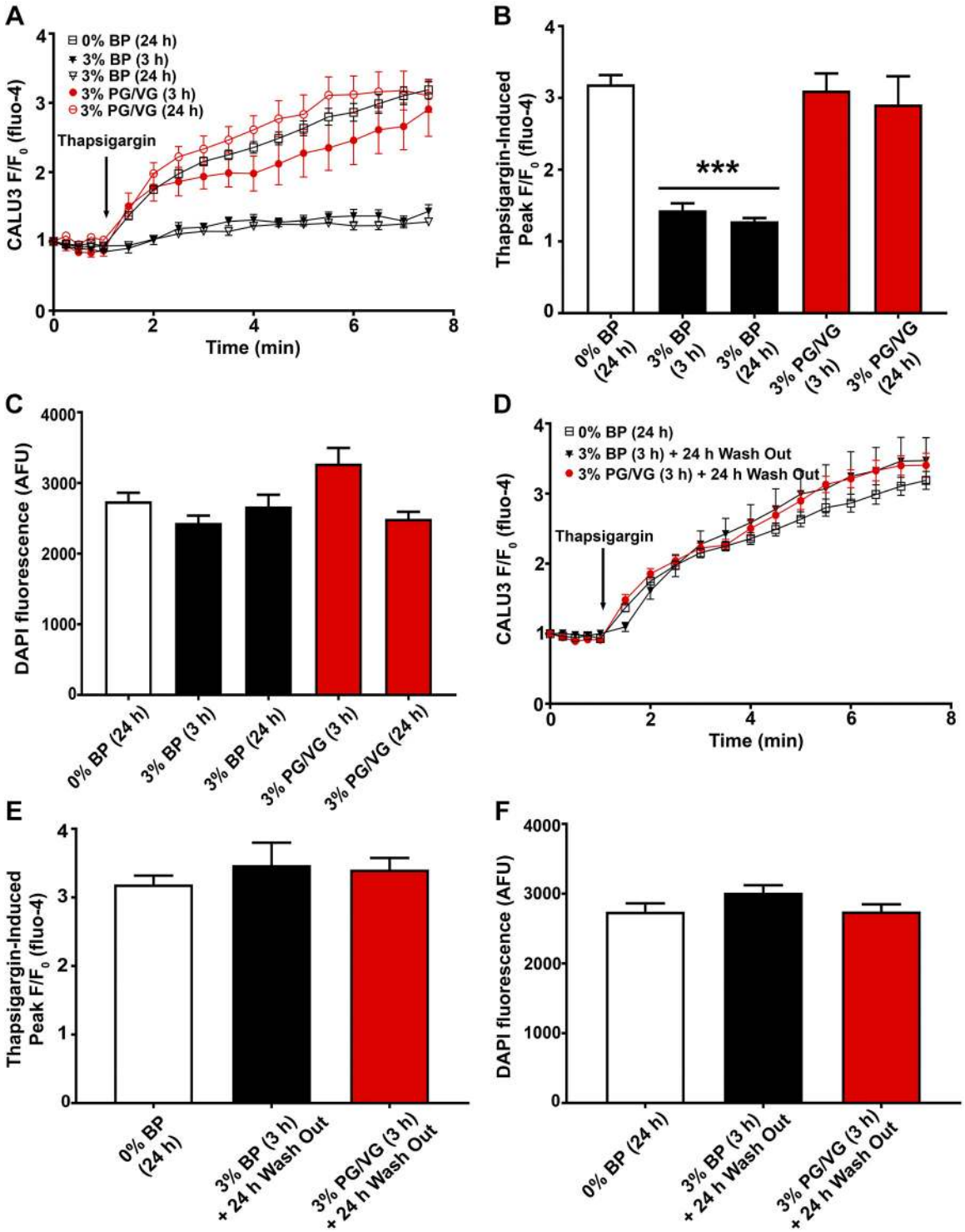

Fig. 4. Pretreatment with Banana Pudding e-liquid (BP) attenuates thapsigargin-induced Ca^{2+} release. CALU3 cells were seeded into 96-well plates and then exposed to 0–3% BP or polyethylene glycol-vegetable glycerin (PG/VG) for 3–24 h. Where indicated, these treatments were washed out and replaced with fresh medium. Cells were then loaded with the Ca^{2+} indicator fluo 4, and medium was replaced with Ringer solution before the cytosolic Ca^{2+} response to thapsigargin was measured. *A*: mean fluo 4 responses to thapsigargin over time after exposure to Ringer solution (0 BP), BP (3 h), BP (24 h), PG/VG (3 h), and PG/VG (24 h). F/F_0, fluorescence ratio. *B*: mean peak thapsigargin-induced fluo 4 responses from *A*. *C*: mean DAPI fluorescence after Ca^{2+} measurements in cells from *A* and *B* that were fixed and stained with DAPI. AFU, arbitrary fluorescence units. *D*: mean fluo 4 responses to thapsigargin over time after exposure to Ringer solution (0 BP), BP (3 h) + 24-h washout, or PG/VG (3 h) + 24-h washout. *E*: mean peak thapsigargin-induced fluo 4 responses taken from *C*. *F*: mean DAPI fluorescence obtained after Ca^{2+} measurements in cells from *A* and *B* that were fixed and stained with DAPI. Values are means ± SE; n = 13–33 wells per treatment. ***$P < 0.001$ vs. control. For *E* and *F*, no differences were found between groups compared with 0% BP/vehicle.

thapsigargin after BP exposure, we tested whether this effect was dependent on the ER/SOCE pathway. We performed Ca^{2+} replacement studies to measure cytosolic Ca^{2+}: cells were placed in Ca^{2+}-free Ringer solution; then, after ER Ca^{2+} was depleted, 2 mM Ca^{2+} was added extracellularly. After this protocol, thapsigargin caused a small peak due to ER Ca^{2+} release that was followed by a second, larger SOCE response when Ca^{2+} was restored extracellularly (Fig. 5*A*). Addition of 3% BP (12 mg/ml nicotine) elicited a similar peak in nominal Ca^{2+}-free solution and a second larger peak in the presence of extracellular Ca^{2+} solution that was thapsigargin-insensitive (Fig. 5*A*). Moreover, pretreatment of cells with thapsigargin abolished the 3% BP Ca^{2+} response (Fig. 5*B*). Together, these data suggest that BP activated a classic ER-dependent SOCE response. The mitochondria are also a significant store of intracellular Ca^{2+} (41). To test for the contributions of mitochondria to the BP Ca^{2+} response, we pretreated cells with CCCP, which caused mitochondrial Ca^{2+} depletion. In CALU3 cells, CCCP pretreatment did not alter the cytosolic Ca^{2+} response to BP (Fig. 5*C*). Additionally, we loaded CALU3 cells with the mitochondrial Ca^{2+} indicator rhod 2 to directly measure mitochondrial Ca^{2+} stores. There was no significant difference in rhod 2 fluorescence following 3% BP or PG/VG compared with vehicle (Fig. 5*D*). As a positive control and to confirm that we were measuring mitochondrial Ca^{2+}, we added the mitochondrial uncoupler CCCP. This compound diminished rhod 2 mitochondrial Ca^{2+} levels, and BP had no additional effect in the presence of CCCP (Fig. 5*D*).

BP induces inositol phosphate formation. Since we found that BP caused ER Ca^{2+} depletion/SOCE, we next sought to identify the underlying mechanism. We previously reported that e-liquids are autofluorescent, especially in the UV excitation range (15). BP was one of the least autofluorescent e-liquids tested in this study and, at the settings used on the epifluorescence microscope and plate reader, did not interfere with the fura 2 or fluo 4 experiments, since it was significantly less bright than either of these dyes. However, BP autofluorescence could be visualized by confocal microscopy at high (405-nm) laser intensities and high photomultiplier tube gain

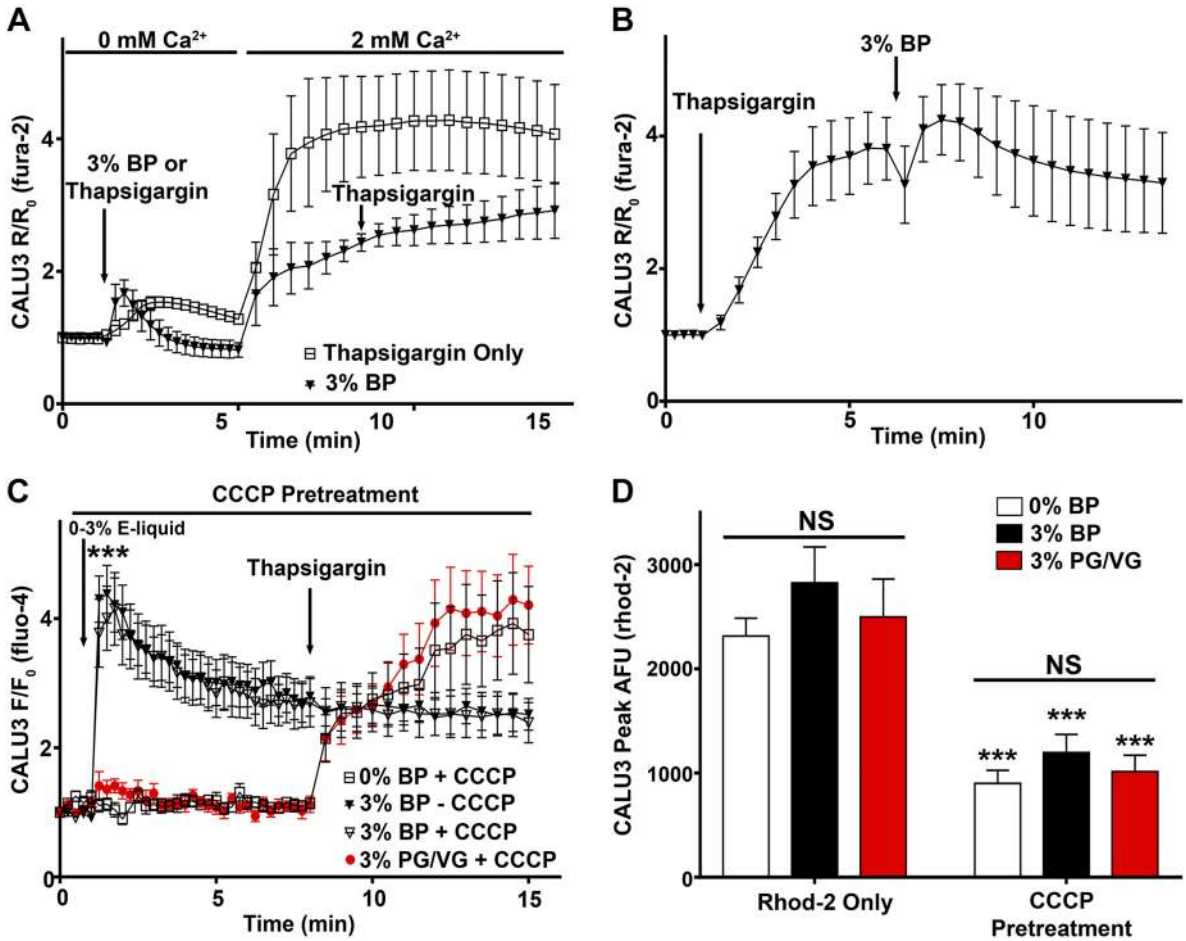

Fig. 5. Ca^{2+} responses to Banana Pudding e-liquid (BP) are endoplasmic reticulum (ER)- and store-operated Ca^{2+} entry (SOCE)-dependent and do not involve mitochondrial Ca^{2+}. *A* and *B*: CALU3 cells were seeded onto glass coverslips and loaded with fura 2. *A*: cells were challenged with BP or polyethylene glycol-vegetable glycerin (PG/VG) diluted in Ringer solution containing nominal (0 mM) or 2 mM Ca^{2+}. Ca^{2+} signal was measured over time and reported as a trace or the peak fluorescence change in response to treatments. *B*: cells were challenged with thapsigargin followed by 3% BP. *C*: CALU3 cells were plated onto 12-well dishes, loaded with fluo 4, and pretreated with or without carbonyl cyanide *m*-chlorophenyl hydrazine (CCCP) before they were exposed to BP or PG/VG diluted in Ringer solution followed by thapsigargin. F/F_0, fluorescence ratio. *D*: CALU3 cells were plated onto 12-well dishes, loaded with the mitochondrial Ca^{2+} indicator rhod 2, and pretreated with or without CCCP before they were exposed to BP or PG/VG diluted in Ringer solution. Peak changes in mitochondrial Ca^{2+} in response to treatments were plotted. AFU, arbitrary fluorescence units. Values are means ± SE; n = 5–6 coverslips per treatment (*A* and *B*) and 7–15 wells per treatment (*C* and *D*). ***$P < 0.001$ vs. control or ± CCCP; NS, not significant.

settings. Therefore, we used this property to test whether BP could enter CALU3 cells in an effort to understand how BP exerted its effects. After addition of 3% BP, confocal microscopy rapidly (<30 s) detected concentrated autofluorescence inside the cells (Fig. 6*A*). Activation of PLC by G_q leads to cleavage of phosphatidylinositol 4,5-biphosphate (PIP_2) and causes Ca^{2+} release after activating the ER's IP_3 receptors. We measured cytosolic Ca^{2+} levels in the presence/absence of the G_q inhibitor YM-254890 (Fig. 6*B*). UTP is a purinergic receptor agonist that also activates G_q/PLC, and the UTP response was attenuated by YM-254890 (Fig. 6*B*). Interestingly, YM-254890 did not inhibit the BP response. To determine whether BP activates PLC, total inositol phosphate accumulation was measured following a 2-min exposure to PG/VG, buffer control, UTP (positive control), or BP with or without 12 mg/ml nicotine. BP significantly increased total inositol phosphate production (percent activation) compared with PG/VG independently of nicotine (Fig. 6*C*). Again, the response was similar to that seen with UTP, which also induces PLC activation following activation of the $P2Y_2$ receptor (16). Since we observed BP-induced PLC activation and subsequent inositol phosphate accumulation, we next exposed HEK-293T cells to the IP_3 receptor antagonist 2-APB (37) to test the involvement of IP_3 formation in eliciting the BP Ca^{2+} response. Representative responses of cytosolic Ca^{2+} to addition of UTP or BP in the presence or absence of 2-APB are shown in Fig. 6*D*. Both UTP and BP significantly elevated cytosolic Ca^{2+} compared with vehicle, and 2-APB pretreatment significantly attenuated both responses (Fig. 6*D*).

BP induces STIM1/Orai1 puncta formation (SOCE) and PKCα phosphorylation. IP_3-dependent ER Ca^{2+} release causes aggregation and relocation of the ER membrane protein STIM1 into discrete puncta at the ER-plasma membrane junction, which activates Orai1 and is required for subsequent plasma membrane Ca^{2+} influx (32, 42). Accordingly, we transfected HEK-293T cells with STIM1-mCherry or Orai1-YFP and

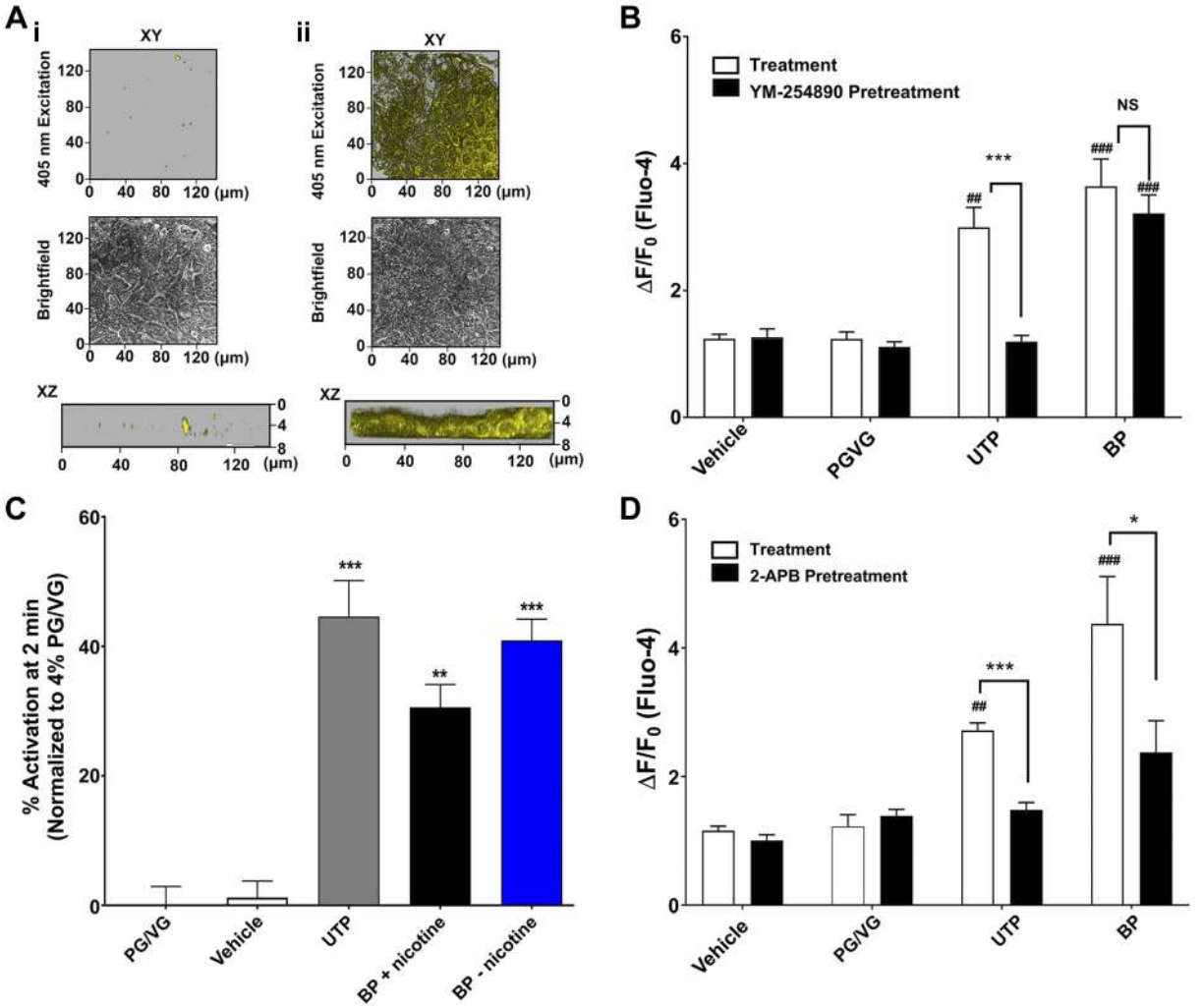

Fig. 6. Banana Pudding e-liquid (BP) activates phospholipase C. *A*: CALU3 cells were imaged by confocal microscopy before (A_i) and 30 s after (A_{ii}) addition of 3% BP to measure intracellular BP accumulation (yellow). Bright-field images (gray) are shown for comparison. *B*: change in fluo 4 fluorescence (F/F_0) in HEK-293T cells. Cells were treated with 10 μM YM-254890 and then with either 100 μM UTP or 1% BP (n = 9–12 replicates per group). *C*: HEK-293T cells seeded on 24-well plates were incubated with [^{3}H]inositol and exposed to 200 μM UTP or 1% BP or polyethylene glycol-vegetable glycerin (PG/VG) for 2 min, and total intracellular inositol phosphate was collected, measured, and plotted as percent activation normalized to 1% PG/VG control. *D*: change in fluo 4 fluorescence in HEK-293T cells. Cells were treated with 100 μM 2-aminoethoxydiphenyl borate (2-APB) followed by either 100 μM UTP or 1% BP. Values are means ± SE. $*P < 0.05$, $**P < 0.01$, $***P < 0.001$ vs. vehicle. $\#\#P < 0.05$, $\#\#\#P < 0.001$ ± UTP or BP.

looked for the puncta formation of these proteins following BP exposure. Transfected cells were treated with 0% BP, thapsigargin, 3% PG/VG, or 3% BP with or without 12 mg/ml nicotine, and both STIM1-mCherry and Orai1-YFP were imaged by confocal microscopy (Fig. 7*A*). 3% BP significantly increased both STIM1 and Orai1 puncta formation to a degree similar to thapsigargin, independent of the presence of nicotine (Fig. 7, *B* and *C*). Downstream of ER/SOCE activation, Ca^{2+} alters the phosphorylation of key protein kinases, which further impacts cell function, including gene expression and protein translation (17, 19). For example, PKCα is canonically activated downstream of IP_3 formation and Ca^{2+} signaling and plays a role in many biological functions (e.g., cell proliferation) (36, 57, 61). We tested whether BP could induce phosphorylation of PKCα. Respective Western blots for phosphorylated PKCα, total PKCα, and GAPDH were generated from CALU3 cells treated with 3% BP (12 mg/ml nicotine) over time (Fig. 7*D*). There was a significant increase in PKCα phosphorylation over time, indicating that BP e-liquid has the ability not only to induce SOCE, but also to phosphorylate important downstream protein kinases (Fig. 7*E*).

DISCUSSION

The major conclusion from this study was that multiple e-liquids affect cell Ca^{2+} homeostasis in a largely nicotine-independent manner. Indeed, we found that 42 of 100 e-liquids elicited a significant Ca^{2+} response (Fig. 1*A*, Table 1). Using the Random Forest model, which compares predictive variables with actual variables (in this case, the change in cytoplasmic Ca^{2+}), we found that the more chemicals that an e-liquid contained, the more likely it was to affect Ca^{2+} signaling (Fig. 1*B*). We previously found that the total number of chemicals in an e-liquid correlated with increased cytotoxicity, suggesting that e-liquids containing more chemicals should be prioritized for future toxicity testing and considered for regulation by the US Food and Drug Administration and other regulatory bodies (50). More specifically, the top-three compounds associated with changes in cytosolic Ca^{2+} were ethyl vanillin, vanillin, and ethyl maltol (Fig. 1*B*), all of which have been commonly found in e-liquids and have the potential to affect cell function (22, 26, 48, 50, 56, 60). Interestingly, ethyl vanillin has been shown to induce IP_3 formation in isolated odorant cilia (51), suggesting that it may affect Ca^{2+} signaling by stimulating PLC. Vanillin is a common flavor that is used in foods. However, while the gastrointestinal tract has a high luminal volume, the airways are surrounded by an extremely thin film of liquid that has a total volume of ~3 mL for the entire lung, and the inhaled concentrations of vanillin and other flavors to which pulmonary cells are exposed may be far greater than the exposure after oral ingestion, potentially leading to a greater cell response. In our analysis, we were able to correctly classify ~75% of the data set. However, the GC-MS data that we used are strictly qualitative and only indicate the presence/absence of a detected chemical, but not its concentration. Thus the model could be improved by determining the concentrations of e-liquid chemical constituents. Unfortunately, accurate determination of chemical concentration by GC-MS relies on the availability of standard materials and is labor-intensive, especially when considering the ever-growing number of available e-liquids.

We previously found that cigarette smoke exposure elicited robust Ca^{2+} responses in primary HBECs, as well as in the CALU3 airway cell line and HEK-293T cells (45). Therefore, we tested the ability of a representative e-liquid, BP, to acutely stimulate Ca^{2+} release in these three cell types. Importantly, the BP Ca^{2+} response was also robust and was seen with direct e-liquid and aerosol addition (Figs. 1–3). Interestingly, while direct e-liquid addition resulted in a typical Ca^{2+} response of transient peak vs. plateau (Figs. 1 and 2), aerosol-induced e-liquid addition gave a more sustained response (Fig. 3). Multiple lines of evidence suggest that BP elicited a classic ER/SOCE-type response. *1*) Pretreatment with BP abolished the effects of the SERCA pump inhibitor thapsigargin (Fig. 4, *A–D*), and vice versa (Fig. 5*B*). *2*) BP still elevated cytoplasmic Ca^{2+} in the absence of extracellular Ca^{2+}, and cytosolic Ca^{2+} increased when extracellular Ca^{2+} was reintroduced (Fig. 5*A*). *3*) No change in Ca^{2+} was detected when cells were labeled with the mitochondrial dye rhod 2 (Fig. 5, *C* and *D*). *4*) BP exposure caused STIM1 and Orai1 to reorganize into puncta (Fig. 7*A–C*), which is indicative of their activation. Here, the effects on STIM1/Orai1 reprised those seen with thapsigargin and were independent of nicotine and PG/VG. Interestingly, cigarette smoke exposure induced a lysosomal Ca^{2+} response that was thapsigargin-insensitive (45), indicating that the cellular response to cigarette smoke differs greatly from the cellular response to e-cigarette vapor. Similarly, the proteomic studies of human bronchial epithelia and airway secretions yield markedly differing results from smokers vs. vapers (23, 46). If we are indeed observing a different and/or novel response in vapers' airways, the long-term health effects of vaping may be less akin to those in tobacco smokers and/or more difficult to predict.

That we observed a Ca^{2+} response after direct e-liquid addition and after vaping suggested that this response was due to the actual e-liquid constituents, and not to metabolites formed by thermal degradation during the vaping process (Figs. 2 and 3). However, the sustained Ca^{2+} response to aerosol exposure suggested that we may have been seeing apoptosis under these conditions. Apoptosis has been detected in e-liquid-exposed alveolar cells and macrophages (6, 52), and apoptosis is concomitant with a sustained Ca^{2+} response (40). Alternatively, it may be that a much lower concentration of e-liquid constituents is seen with each aerosol puff than when the e-liquid is added directly. Thus the lower level of exposure by aerosol may lead to a more constant, but smaller, increase in Ca^{2+} release without inducing desensitization, allowing for a more persistent signal. We previously observed a lack of Ca^{2+} desensitization when airway epithelia were exposed to phasic shear stress. Shear stress releases extremely low (nanomolar) levels of ATP into the mucosal compartment that are sufficient to stimulate a Ca^{2+} signal without desensitization (59). Understanding whether e-liquids can induce SOCE and/or apoptosis, depending on the dose and delivery method, will be critical in understanding the potential health impact of vaping. Unfortunately, real-world vaping patterns vary greatly, driven in part by the wide variety of e-liquids, nicotine concentrations, and devices that are commercially available. For example, in a recent study of vapers, we found that the average number of puffs per day varied from 7 to 265, depending on the subject (23). For our studies, we chose to administer 5–25 puffs, which was on the lower end of real-world vaping. Given

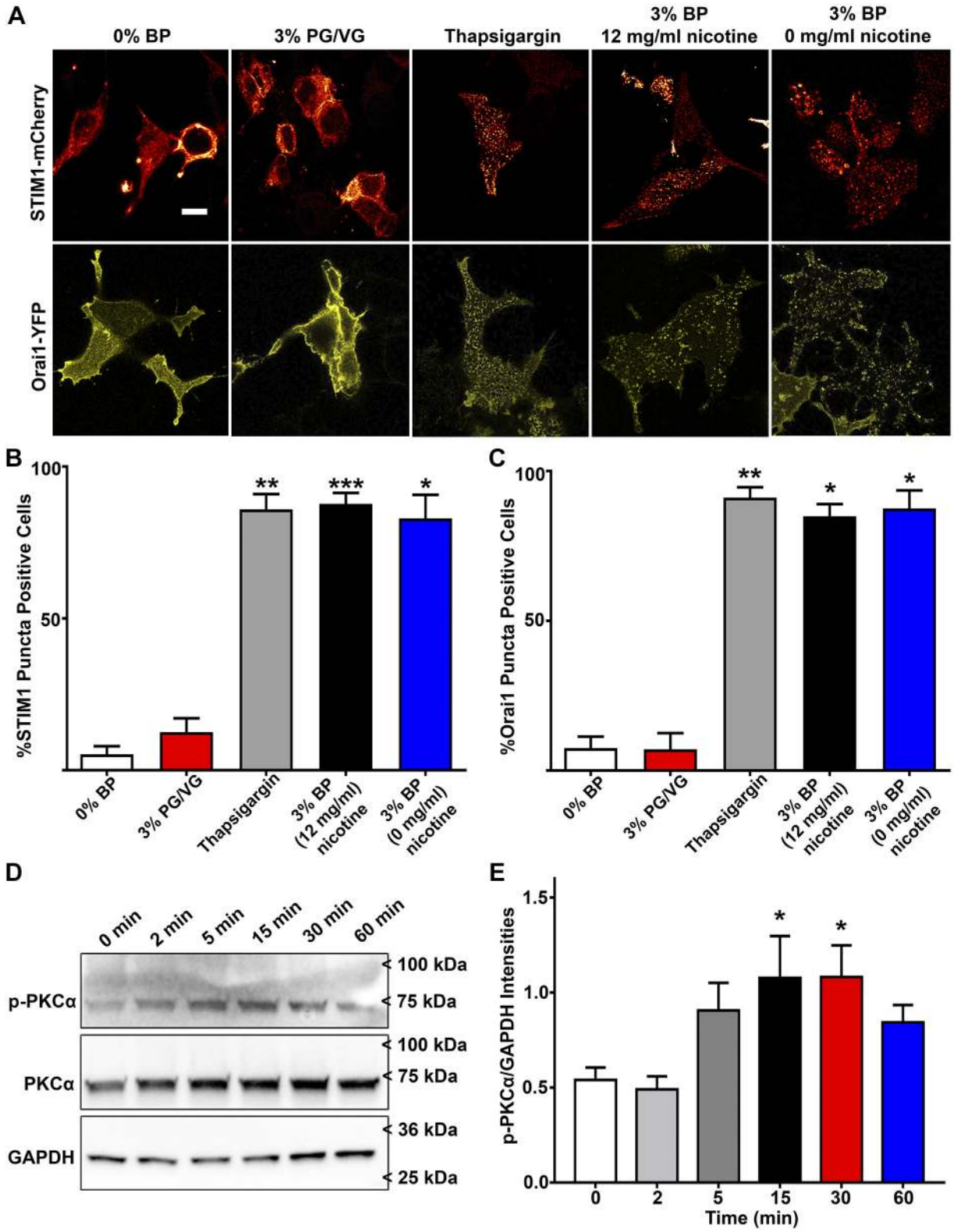

Fig. 7. Exposure to Banana Pudding e-liquid (BP) induces stromal interaction molecule 1 (STIM1)/Orai1 puncta formation and protein kinase Cα (PKCα) phosphorylation. *A–C*: transfected HEK-293T cells were exposed to 0% BP (medium only), 3% polyethylene glycol-vegetable glycerin (PG/VG), thapsigargin, or 3% BP with or without 12 mg/ml nicotine for 5–10 min. Cells were fixed and imaged, and percentage of puncta-positive cells was measured for STIM1-mCherry and Orai1-yellow fluorescent protein (YFP). Scale bar = 25 μm. *D* and *E*: CALU3 cells were seeded into 60-mm dishes and treated with 3% BP diluted in medium for 0–60 min. Protein lysates were collected, and immunoblots were performed for phosphorylated PKCα (p-PKCα), total PKCα, and GAPDH (loading control). Representative blots of all proteins with treatment are shown. Band intensities were measured, and the ratio of p-PKCα to GAPDH was plotted. Values are means ± SE; n = 4–9 coverslips per treatment (*B* and *C*) and 6 blots per time point (*E*). $^{*}P < 0.05$, $^{**}P < 0.01$, $^{***}P < 0.001$ vs. 0% BP control or 0-min time point.

that we waited 30 s between each puff, we believed that this was an achievable protocol. However, further cellular studies are needed to understand the implications of these doses and to better understand the relative acute vs. chronic effects of vaping.

To date, no other study has shown the ability of e-liquids to stimulate ER Ca^{2+} release/SOCE. IP_3-dependent oscillations in the cytoplasmic Ca^{2+} signal have been described in airway epithelia and in other cells (11, 38). These repetitive cytoplasmic Ca^{2+} transients may indicate digital signaling (10). We previously showed that tobacco smoke-induced Ca^{2+} responses are relatively slow-changing, but persistent, signals (45). Therefore, in our studies we sampled fura 2 and fluo 4 fluorescence every 30 s to avoid dye photobleaching over extended measurement periods. However, a limitation of our approach is that we may have missed rapid changes in the Ca^{2+} signal, including Ca^{2+} transients and/or oscillations. Thus, further studies are required to fully understand whether e-liquids such as BP can induce Ca^{2+} oscillations.

Bitter and sweet taste receptors are GPCRs that are expressed not only in olfactory tissues, but also in the airways (2). We initially hypothesized that taste receptors might be activated by e-liquids, since e-liquids often contain sweet flavors to mask the bitter taste of nicotine. Using quantitative PCR analysis, we found little or no expression of several taste receptor isoforms or their associated G protein (Gα-gustducin) in HBECs, CALU3 cells, or HEK-293T cells (data not shown), suggesting that this effect was not taste receptor-mediated. However, it is possible that other, as-yet-unidentified GPCRs were activated directly by components of BP and other e-liquids. We previously showed that the autofluorescent e-liquid Pixie Dust can rapidly enter HEK-293T cells and polarized airway epithelia (23). Similarly, BP rapidly entered CALU3 cells (Fig. 6*A*) and, rather than stimulate a GPCR, may have intracellularly activated G_q or PLC. Indeed, we found that the G_q antagonist YM-254890 was not able to inhibit the BP-induced Ca^{2+} response, although it did inhibit the UTP response (Fig. 6*B*). PLC is an enzyme that is associated with the inner face of the plasma membrane that cleaves phospholipids such as PIP_2 to form IP_3 (9), and our data indicate that BP activated PLC/induced inositol phosphate formation that was *1*) PG-, VG-, and nicotine-independent and *2*) equal in magnitude to inositol phosphate formation induced by UTP (Fig. 6*C*). Interestingly, PLC can be directly activated by small molecules. For example, *N*-(3-trifluoromethylphenyl)-2,4,6-trimethylbenzenesulfonamide acutely activates PLC, leading to increases in cytosolic Ca^{2+}, independent of G_q stimulation (5). Further experiments are needed to better understand the effect of BP and similar flavors on G_q/PLC-mediated cell signaling and to determine which component of this pathway they activate. However, consistent with these observations, the IP_3 receptor antagonist 2-APB abolished both UTP- and BP-induced increases in cytosolic Ca^{2+} (Fig. 6*D*). 2-APB can also affect transient receptor potential (TRP) channels (35). However, given that this was an ER-dependent Ca^{2+} response, it is unlikely that we were observing TRP channel-mediated effects (see below).

Other common flavors can activate TRP channels. For example, menthol was found in two flavors that also increased cytoplasmic Ca^{2+} (i.e., Arctic Tobacco and Menthol) (Fig. 1*A*, Table 1) and was in our list of 27 chemicals associated with changes in cytoplasmic Ca^{2+} (Fig. 1*B*). Thus, while it is likely that menthol in the Menthol and Arctic Tobacco flavors activated TRP channels to increase cytosolic Ca^{2+}, since BP stimulated ER Ca^{2+} release in the absence of extracellular Ca^{2+} (Fig. 5*A*), it acts, at least in part, independently of TRP channels. The BP Ca^{2+} response was also nicotine-independent, but its duration was increased when nicotine was present (Fig. 2, *E–H*). We previously measured the Ca^{2+} response to nicotine in CALU3 cells. In this cell line, CHRNA5 is the only nicotinic acetylcholine receptor to be expressed, and the nicotine EC_{50} to elicit a response was ~6 mM (48), suggesting that this is a nonspecific response to high levels of nicotine. Nevertheless, a dose of this magnitude has pathological relevance during inhalation, given that levels of nicotine can exceed 100 mM in e-liquids.

Activation of PLC and subsequent IP_3 formation/Ca^{2+} signaling constitute a normal physiological response to G_q-linked GPCR stimulation (9, 16). However, in the healthy lung, this response typically occurs after exposure to relatively low levels of agonist. For example, the purine nucleotide ATP, which activates G_q-linked P2Y receptors, is typically present at submicromolar levels in lung lining fluid, even though it can show effects at up to 100 μM pharmacologically (58). Thus, chronic activation of PLC by BP or similarly flavored e-liquids that contain high levels of agonists may have the potential to trigger aberrant downstream responses. For example, Ca^{2+}-sensitive transcription factors may be activated, or there may be Ca^{2+}-mediated activation of cell division, cell growth and apoptosis, or ER stress caused by chronic depletion of ER Ca^{2+}, which can lead to an unfolded protein response, cell apoptosis, or chronic inflammation (20, 47). Furthermore, increased MUC5AC mucin and protease levels and NETosis have been observed in vapers' sputum (46). Interestingly, all these processes can be Ca^{2+}-dependent (1, 14, 28), and it is possible that e-liquid/vape-induced elevations in cytosolic Ca^{2+} contribute to the increased secretion of proteases, mucins, and NETosis. Increased secretions of mucins and other macromolecules have been proposed as potential biomarkers of harm in the airways (3, 12).

The study of e-cigarettes is relatively new, although we acknowledge that the study of flavors, many of which are aldehydes that can form adducts with proteins, is not new per se. Importantly, our data illustrates that the mechanisms underlying the effects of vaping can be determined and provide further focus for future studies. We previously found that STIM1, the ER Ca^{2+}-sensing protein, is upregulated in vapers' airways (23), suggesting that altered Ca^{2+} homeostasis may occur in chronic vapers. Indeed, given the importance of Ca^{2+} signaling in normal cell physiology, we propose that the impact of e-liquids on Ca^{2+} be further investigated in vivo and prioritized in high-throughput screens when assessing the effects of e-liquids in vitro.

GRANTS

This study was funded by the University of North Carolina School of Medicine Tobacco Center of Regulatory Science (TCORS) and National Heart, Lung, and Blood Institute Grants P50-HL-120100-01 and R01-HL-135642. This research was supported in part by the Intramural Research Program of the National Institute of Environmental Health Sciences.

DISCLAIMERS

Research reported in this publication was supported by the National Institutes of Health (NIH) and the Family Smoking Prevention and Tobacco Control Act. The content is solely the responsibility of the authors and does not necessarily represent the official views of the NIH or the US Food and Drug Administration.

DISCLOSURES

No conflicts of interest, financial or otherwise, are declared by the authors.

AUTHOR CONTRIBUTIONS

T.R.R., J.E.K., G.L.G., S.B.S., and R.T. conceived and designed research; T.R.R., J.E.K., and S.B.S. performed experiments; T.R.R., J.E.K., B.T.Z., G.L.G., S.B.S., and R.T. analyzed data; T.R.R., J.E.K., B.T.Z., G.L.G., S.B.S., and R.T. interpreted results of experiments; T.R.R., B.T.Z., and R.T. prepared figures; T.R.R. and R.T. drafted manuscript; T.R.R., B.T.Z., G.L.G., S.B.S., and R.T. edited and revised manuscript; T.R.R., J.E.K., B.T.Z., G.L.G., S.B.S., and R.T. approved final version of manuscript.

REFERENCES

1. **Adler KB, Tuvim MJ, Dickey BF.** Regulated mucin secretion from airway epithelial cells. *Front Endocrinol (Lausanne)* 4: 129, 2013. doi:10.3389/fendo.2013.00129.
2. **An SS, Liggett SB.** Taste and smell GPCRs in the lung: evidence for a previously unrecognized widespread chemosensory system. *Cell Signal* 41: 82–88, 2018. doi:10.1016/j.cellsig.2017.02.002.
3. **Anderson WH, Coakley RD, Button B, Henderson AG, Zeman KL, Alexis NE, Peden DB, Lazarowski ER, Davis CW, Bailey S, Fuller F, Almond M, Qaqish B, Bordonali E, Rubinstein M, Bennett WD, Kesimer M, Boucher RC.** The relationship of mucus concentration (hydration) to mucus osmotic pressure and transport in chronic bronchitis. *Am J Respir Crit Care Med* 192: 182–190, 2015. doi:10.1164/rccm.201412-2230OC.
4. **Arrazola RA, Singh T, Corey CG, Husten CG, Neff LJ, Apelberg BJ, Bunnell RE, Choiniere CJ, King BA, Cox S, McAfee T, Caraballo RS; Centers for Disease Control and Prevention (CDC).** Tobacco use among middle and high school students—United States, 2011–2014. *MMWR Morb Mortal Wkly Rep* 64: 381–385, 2015.
5. **Bae YS, Lee TG, Park JC, Hur JH, Kim Y, Heo K, Kwak JY, Suh PG, Ryu SH.** Identification of a compound that directly stimulates phospholipase C activity. *Mol Pharmacol* 63: 1043–1050, 2003. doi:10.1124/mol.63.5.1043.
6. **Bahmed K, Lin CR, Simborio H, Karim L, Aksoy M, Kelsen S, Tomar D, Madesh M, Elrod J, Messier E, Mason R, Unterwald EM, Eisenstein TK, Criner GJ, Kosmider B.** The role of DJ-1 in human primary alveolar type II cell injury induced by e-cigarette aerosol. *Am J Physiol Lung Cell Mol Physiol* 317: L475–L485, 2019. doi:10.1152/ajplung.00567.2018.
7. **Barrington-Trimis JL, Samet JM, McConnell R.** Flavorings in electronic cigarettes: an unrecognized respiratory health hazard? *JAMA* 312: 2493–2494, 2014. doi:10.1001/jama.2014.14830.
8. **Behar RZ, Wang Y, Talbot P.** Comparing the cytotoxicity of electronic cigarette fluids, aerosols and solvents. *Tob Control* 27: 325–333, 2018. doi:10.1136/tobaccocontrol-2016-053472.
9. **Berridge MJ.** Inositol trisphosphate and calcium signalling mechanisms. *Biochim Biophys Acta* 1793: 933–940, 2009. doi:10.1016/j.bbamcr.2008.10.005.
10. **Bird GS, Hwang SY, Smyth JT, Fukushima M, Boyles RR, Putney JW Jr.** STIM1 is a calcium sensor specialized for digital signaling. *Curr Biol* 19: 1724–1729, 2009. doi:10.1016/j.cub.2009.08.022.
11. **Boitano S, Dirksen ER, Sanderson MJ.** Intercellular propagation of calcium waves mediated by inositol trisphosphate. *Science* 258: 292–295, 1992. doi:10.1126/science.1411526.
12. **Chalmers JD, Moffitt KL, Suarez-Cuartin G, Sibila O, Finch S, Furrie E, Dicker A, Wrobel K, Elborn JS, Walker B, Martin SL, Marshall SE, Huang JT, Fardon TC.** Neutrophil elastase activity is associated with exacerbations and lung function decline in bronchiectasis. *Am J Respir Crit Care Med* 195: 1384–1393, 2017. doi:10.1164/rccm.201605-1027OC.
13. **Chen J, Sanderson MJ.** Store-operated calcium entry is required for sustained contraction and Ca^{2+} oscillations of airway smooth muscle. *J Physiol* 595: 3203–3218, 2017. doi:10.1113/JP272694.
14. **Cohen JR, Faust G, Tenenbaum N, Sarfati I, Rogowsky P, Wise L.** The calcium messenger system and the kinetics of elastase release from human neutrophils in patients with abdominal aortic aneurysms. *Ann Vasc Surg* 4: 570–574, 1990. doi:10.1016/S0890-5096(06)60841-8.
15. **Davis ES, Sassano MF, Goodell H, Tarran R.** E-liquid autofluorescence can be used as a marker of vaping deposition and third-hand vape exposure. *Sci Rep* 7: 7459, 2017. doi:10.1038/s41598-017-07862-w.
16. **Dickson EJ, Falkenburger BH, Hille B.** Quantitative properties and receptor reserve of the IP_3 and calcium branch of G_q-coupled receptor signaling. *J Gen Physiol* 141: 521–535, 2013. doi:10.1085/jgp.201210886.
17. **Dolmetsch RE, Xu K, Lewis RS.** Calcium oscillations increase the efficiency and specificity of gene expression. *Nature* 392: 933–936, 1998. doi:10.1038/31960.
18. **Enomoto M, Nishikawa T, Siddiqui N, Chung S, Ikura M, Stathopulos PB.** From stores to sinks: structural mechanisms of cytosolic calcium regulation. *Adv Exp Med Biol* 981: 215–251, 2017. doi:10.1007/978-3-319-55858-5_10.
19. **Enslen H, Tokumitsu H, Stork PJ, Davis RJ, Soderling TR.** Regulation of mitogen-activated protein kinases by a calcium/calmodulin-dependent protein kinase cascade. *Proc Natl Acad Sci USA* 93: 10803–10808, 1996. doi:10.1073/pnas.93.20.10803.
20. **Ferri KF, Kroemer G.** Organelle-specific initiation of cell death pathways. *Nat Cell Biol* 3: E255–E263, 2001. doi:10.1038/ncb1101-e255.
21. **Garge NR, Bobashev G, Eggleston B.** Random forest methodology for model-based recursive partitioning: the mobForest package for R. *BMC Bioinformatics* 14: 125, 2013. doi:10.1186/1471-2105-14-125.
22. **Gerloff J, Sundar IK, Freter R, Sekera ER, Friedman AE, Robinson R, Pagano T, Rahman I.** Inflammatory response and barrier dysfunction by different e-cigarette flavoring chemicals identified by gas chromatography-mass spectrometry in e-liquids and e-vapors on human lung epithelial cells and fibroblasts. *Appl In Vitro Toxicol* 3: 28–40, 2017. doi:10.1089/aivt.2016.0030.
23. **Ghosh A, Coakley RC, Mascenik T, Rowell TR, Davis ES, Rogers K, Webster MJ, Dang H, Herring LE, Sassano MF, Livraghi-Butrico A, Van Buren SK, Graves LM, Herman MA, Randell SH, Alexis NE, Tarran R.** Chronic e-cigarette exposure alters the human bronchial epithelial proteome. *Am J Respir Crit Care Med* 198: 67–76, 2018. doi:10.1164/rccm.201710-2033OC.
24. **Harrell MB, Weaver SR, Loukas A, Creamer M, Marti CN, Jackson CD, Heath JW, Nayak P, Perry CL, Pechacek TF, Eriksen MP.** Flavored e-cigarette use: characterizing youth, young adult, and adult users. *Prev Med Rep* 5: 33–40, 2017. doi:10.1016/j.pmedr.2016.11.001.
25. **Hsu G, Sun JY, Zhu SH.** Evolution of electronic cigarette brands from 2013–2014 to 2016–2017: analysis of brand websites. *J Med Internet Res* 20: e80, 2018. doi:10.2196/jmir.8550.
26. **Hutzler C, Paschke M, Kruschinski S, Henkler F, Hahn J, Luch A.** Chemical hazards present in liquids and vapors of electronic cigarettes. *Arch Toxicol* 88: 1295–1308, 2014. doi:10.1007/s00204-014-1294-7.
27. **Immler R, Simon SI, Sperandio M.** Calcium signalling and related ion channels in neutrophil recruitment and function. *Eur J Clin Invest* 48, *Suppl* 2: e12964, 2018. doi:10.1111/eci.12964.
28. **Kenny EF, Herzig A, Krüger R, Muth A, Mondal S, Thompson PR, Brinkmann V, Bernuth HV, Zychlinsky A.** Diverse stimuli engage different neutrophil extracellular trap pathways. *eLife* 6: e24437, 2017. doi:10.7554/eLife.24437.
29. **Kishimoto A, Takai Y, Mori T, Kikkawa U, Nishizuka Y.** Activation of calcium and phospholipid-dependent protein kinase by diacylglycerol, its possible relation to phosphatidylinositol turnover. *J Biol Chem* 255: 2273–2276, 1980.
30. **Kreiss K, Gomaa A, Kullman G, Fedan K, Simoes EJ, Enright PL.** Clinical bronchiolitis obliterans in workers at a microwave-popcorn plant. *N Engl J Med* 347: 330–338, 2002. doi:10.1056/NEJMoa020300.
31. **Lee YH, Gawron M, Goniewicz ML.** Changes in puffing behavior among smokers who switched from tobacco to electronic cigarettes. *Addict Behav* 48: 1–4, 2015. doi:10.1016/j.addbeh.2015.04.003.
32. **Liou J, Kim ML, Heo WD, Jones JT, Myers JW, Ferrell JE Jr, Meyer T.** STIM is a Ca^{2+} sensor essential for Ca^{2+}-store-depletion-triggered Ca^{2+} influx. *Curr Biol* 15: P1235–1241, 2005. doi:10.1016/j.cub.2005.05.055.
33. **Lopez AA, Hiler MM, Soule EK, Ramôa CP, Karaoghlanian NV, Lipato T, Breland AB, Shihadeh AL, Eissenberg T.** Effects of electronic cigarette liquid nicotine concentration on plasma nicotine and puff topography in tobacco cigarette smokers: a preliminary report. *Nicotine Tob Res* 18: 720–723, 2016. doi:10.1093/ntr/ntv182.

34. **Lytton J, Westlin M, Hanley MR.** Thapsigargin inhibits the sarcoplasmic or endoplasmic reticulum Ca-ATPase family of calcium pumps. *J Biol Chem* 266: 17067–17071, 1991.
35. **Ma HT, Patterson RL, van Rossum DB, Birnbaumer L, Mikoshiba K, Gill DL.** Requirement of the inositol trisphosphate receptor for activation of store-operated Ca^{2+} channels. *Science* 287: 1647–1651, 2000. doi:10.1126/science.287.5458.1647.
36. **Mandil R, Ashkenazi E, Blass M, Kronfeld I, Kazimirsky G, Rosenthal G, Umansky F, Lorenzo PS, Blumberg PM, Brodie C.** Protein kinase Cα and protein kinase Cδ play opposite roles in the proliferation and apoptosis of glioma cells. *Cancer Res* 61: 4612–4619, 2001.
37. **Maruyama T, Kanaji T, Nakade S, Kanno T, Mikoshiba K.** 2APB, 2-aminoethoxydiphenyl borate, a membrane-penetrable modulator of Ins(1,4,5)P_3-induced Ca^{2+} release. *J Biochem* 122: 498–505, 1997. doi:10.1093/oxfordjournals.jbchem.a021780.
38. **Muallem S, Zhao H, Mayer E, Sachs G.** Regulation of intracellular calcium in epithelial cells. *Semin Cell Biol* 1: 305–310, 1990.
39. **Park CY, Hoover PJ, Mullins FM, Bachhawat P, Covington ED, Raunser S, Walz T, Garcia KC, Dolmetsch RE, Lewis RS.** STIM1 clusters and activates CRAC channels via direct binding of a cytosolic domain to Orai1. *Cell* 136: 876–890, 2009. doi:10.1016/j.cell.2009.02.014.
40. **Pinton P, Giorgi C, Siviero R, Zecchini E, Rizzuto R.** Calcium and apoptosis: ER-mitochondria Ca^{2+} transfer in the control of apoptosis. *Oncogene* 27: 6407–6418, 2008. doi:10.1038/onc.2008.308.
41. **Prakash YS, Pabelick CM, Sieck GC.** Mitochondrial dysfunction in airway disease. *Chest* 152: 618–626, 2017. doi:10.1016/j.chest.2017.03.020.
42. **Prakriya M, Feske S, Gwack Y, Srikanth S, Rao A, Hogan PG.** Orai1 is an essential pore subunit of the CRAC channel. *Nature* 443: 230–233, 2006. doi:10.1038/nature05122.
43. **Putney JW Jr.** Recent breakthroughs in the molecular mechanism of capacitative calcium entry (with thoughts on how we got here). *Cell Calcium* 42: 103–110, 2007. doi:10.1016/j.ceca.2007.01.011.
44. **Randell SH, Fulcher ML, O'Neal W, Olsen JC.** Primary epithelial cell models for cystic fibrosis research. *Methods Mol Biol* 742: 285–310, 2011. doi:10.1007/978-1-61779-120-8_18.
45. **Rasmussen JE, Sheridan JT, Polk W, Davies CM, Tarran R.** Cigarette smoke-induced Ca^{2+} release leads to cystic fibrosis transmembrane conductance regulator (CFTR) dysfunction. *J Biol Chem* 289: 7671–7681, 2014. doi:10.1074/jbc.M113.545137.
46. **Reidel B, Radicioni G, Clapp PW, Ford AA, Abdelwahab S, Rebuli ME, Haridass P, Alexis NE, Jaspers I, Kesimer M.** E-cigarette use causes a unique innate immune response in the lung, involving increased neutrophilic activation and altered mucin secretion. *Am J Respir Crit Care Med* 197: 492–501, 2018. doi:10.1164/rccm.201708-1590OC.
47. **Ribeiro CM, O'Neal WK.** Endoplasmic reticulum stress in chronic obstructive lung diseases. *Curr Mol Med* 12: 872–882, 2012. doi:10.2174/156652412801318791.
48. **Rowell TR, Reeber SL, Lee SL, Harris RA, Nethery RC, Herring AH, Glish GL, Tarran R.** Flavored e-cigarette liquids reduce proliferation and viability in the CALU3 airway epithelial cell line. *Am J Physiol Lung Cell Mol Physiol* 313: L52–L66, 2017. doi:10.1152/ajplung.00392.2016.
49. **Rowell TR, Tarran R.** Will chronic e-cigarette use cause lung disease? *Am J Physiol Lung Cell Mol Physiol* 309: L1398–L1409, 2015. doi:10.1152/ajplung.00272.2015.
50. **Sassano MF, Davis ES, Keating JE, Zorn BT, Kochar TK, Wolfgang MC, Glish GL, Tarran R.** Evaluation of e-liquid toxicity using an open-source high-throughput screening assay. *PLoS Biol* 16: e2003904, 2018. doi:10.1371/journal.pbio.2003904.
51. **Schandar M, Laugwitz KL, Boekhoff I, Kroner C, Gudermann T, Schultz G, Breer H.** Odorants selectively activate distinct G protein subtypes in olfactory cilia. *J Biol Chem* 273: 16669–16677, 1998. doi:10.1074/jbc.273.27.16669.
52. **Scott A, Lugg ST, Aldridge K, Lewis KE, Bowden A, Mahida RY, Grudzinska FS, Dosanjh D, Parekh D, Foronjy R, Sapey E, Naidu B, Thickett DR.** Pro-inflammatory effects of e-cigarette vapour condensate on human alveolar macrophages. *Thorax* 73: 1161–1169, 2018. doi:10.1136/thoraxjnl-2018-211663.
53. **Shaw PJ, Feske S.** Regulation of lymphocyte function by ORAI and STIM proteins in infection and autoimmunity. *J Physiol* 590: 4157–4167, 2012. doi:10.1113/jphysiol.2012.233221.
54. **Shears SB.** Measurement of inositol phosphate turnover in intact cells and cell-free systems. In: *Signalling by Inositides: A Practical Approach*, edited by Shears SB. Oxford, UK: Oxford University Press, 1997, p. 33–52.
55. **Sheridan JT, Gilmore RC, Watson MJ, Archer CB, Tarran R.** 17β-Estradiol inhibits phosphorylation of stromal interaction molecule 1 (STIM1) protein: implication for store-operated calcium entry and chronic lung diseases. *J Biol Chem* 288: 33509–33518, 2013. doi:10.1074/jbc.M113.486662.
56. **Sherwood CL, Boitano S.** Airway epithelial cell exposure to distinct e-cigarette liquid flavorings reveals toxicity thresholds and activation of CFTR by the chocolate flavoring 2,5-dimethypyrazine. *Respir Res* 17: 57, 2016. doi:10.1186/s12931-016-0369-9.
57. **Takai Y, Kishimoto A, Iwasa Y, Kawahara Y, Mori T, Nishizuka Y, Tamura A, Fujii T.** A role of membranes in the activation of a new multifunctional protein kinase system. *J Biochem* 86: 575–578, 1979. doi:10.1093/oxfordjournals.jbchem.a132557.
58. **Tarran R, Button B, Boucher RC.** Regulation of normal and cystic fibrosis airway surface liquid volume by phasic shear stress. *Annu Rev Physiol* 68: 543–561, 2006. doi:10.1146/annurev.physiol.68.072304.112754.
59. **Tarran R, Button B, Picher M, Paradiso AM, Ribeiro CM, Lazarowski ER, Zhang L, Collins PL, Pickles RJ, Fredberg JJ, Boucher RC.** Normal and cystic fibrosis airway surface liquid homeostasis. The effects of phasic shear stress and viral infections. *J Biol Chem* 280: 35751–35759, 2005. doi:10.1074/jbc.M505832200.
60. **Tierney PA, Karpinski CD, Brown JE, Luo W, Pankow JF.** Flavour chemicals in electronic cigarette fluids. *Tob Control* 25: e10–e15, 2016. doi:10.1136/tobaccocontrol-2014-052175.
61. **Ways DK, Kukoly CA, deVente J, Hooker JL, Bryant WO, Posekany KJ, Fletcher DJ, Cook PP, Parker PJ.** MCF-7 breast cancer cells transfected with protein kinase Cα exhibit altered expression of other protein kinase C isoforms and display a more aggressive neoplastic phenotype. *J Clin Invest* 95: 1906–1915, 1995. doi:10.1172/JCI117872.